Renewable Energy 160 (2020): 623-632

DOI: https://doi.org/10.1016/j.renene.2020.07.003

Energy valorization of cow manure by hydrothermal carbonization and anaerobic digestion

J.D. Marin-Batista[a], J. Villamil[a], S.V. Qaramaleki[b], C.J. Coronella[b], A.F. Mohedano[a], M.A. de la Rubia[a,*]

[a] Department of Chemical Engineering, Universidad Autonoma de Madrid, Campus de Cantoblanco, 28049, Madrid, Spain.

[b] Department of Chemical and Materials Engineering, University of Nevada, Reno, Reno, 89557, Nevada, United States

*angeles.delarubia@uam.es

Abstract

The work evaluates the energy recovery from hydrothermal carbonization (HTC) of cow manure through the thermal analysis of hydrochar and the anaerobic digestion (AD) of the process water (PW). The increase of the HTC temperature in the range of 170–230ºC improved solid-fuel properties (higher heating value (16.4–20.1 MJ kg^{-1}), fuel ratio (0.19–0.33)) of dairy manure, but less energy can be recovered by its combustion ascribing to reduction of hydrochar yield (65.0–54.0%). Fixed carbon content (12.5–18.7%), and ignition (263–278ºC) and burnout (581–619ºC) temperatures increased with carbonization temperature, thereby reducing risks of fire and explosion. However, the highest value of the comprehensive combustion index, related with good fuel characteristics, was obtained for the hydrochar carbonized at 170ºC. The high organic matter content of the PW allows energy recovery by AD, obtaining the highest methane yield for the PW generated at 170ºC (294±2 mL STP CH_4 g^{-1} VS_{added}). HTC led to higher energy recovery than conventional AD of dairy manure (4.1 MJ kg^{-1}). The energy recovery by AD combined with the energy content of the hydrochar (13.7 MJ kg^{-1}

feedstock for HTC conditions below 200ºC) accounted around 85% of the total energy content of feedstock, allowing a potential valorization route for dairy manure.

Keywords: anaerobic digestion, combustion, dairy manure, hydrothermal carbonization.

1. Introduction

The rapid development of animal husbandry towards high-density animal feeding operations has posed a challenge of proper disposal and utilization for livestock manures (Dai et al., 2017). In the European Union (EU), about 1.4 billion t of livestock manure and animal related wastes is produced each year, specially dairy manure that accounts for 58 % of the net amount (Cherrier et al., 2014). Livestock manures have been traditionally composted and utilized as soil amendments in areas surrounding the place of origin because its transportation to croplands is not cost-effective (Zhou et al., 2019). However, agronomic applications have been under environmental and economic pressure as manure production within intensive farming operations far exceeds local soil demands, often resulting in accumulation and therefore storage (Toufiq Reza et al., 2016). Long-term storage of manure facilitates emission of greenhouse gases (Xiong et al., 2019) and leaching of nitrates and phosphates, giving rise to social and environmental problems such as eutrophication of water sources, proliferation of odors or pathogens (Ghanim et al., 2016).

The effective utilization of livestock manures as bioenergy feedstock has not only alleviated the pressure on providing clean energy, but also reduced the environmental impacts of livestock manure mismanagement (Zhou et al., 2019). Anaerobic digestion (AD) is a common valorization route for animal manures whose treatment capacity has

been extended throughout the EU from 10^5 t y^{-1} in 1990 to $46 \cdot 10^6$ t y^{-1} in 2016 (EBA, 2017; Ecoprog, 2017). AD allows manures stabilization and odor control with simultaneous production of biogas, which it is used to fuel combined heat and power (CHP) systems (Ekpo et al., 2016). However, the low biogas yield of manure hampers the profitability of CHP systems for small to medium farms. Imeni et al. (2019) carried out techno-economic assessments on AD of dairy manure showing that for a medium-size farm with 250 adult cattle heads, the revenues generated by the AD process are not able to offset the initial required investment. On the other hand, the energy obtained from 1 t of dry livestock is comparable to the energy of 0.375 t of fossil coal (Wu et al., 2018), which brings up the idea of using livestock manures as a potential solid-fuel. Nevertheless, there are some drawbacks for direct combustion of animal manure such as high moisture content (60 – 90 %), low higher heating value (HHV; 14 – 16 MJ kg^{-1}), and poor dewaterability and grindability (Gao et al., 2018; Tavasoli et al., 2018), often resulting in low energy efficiencies and high operation costs (Lang et al., 2019a). These serious obstacles can be addressed with innovative environmental management approaches, such as thermal treatments which have emerged as promising technologies to target resource recovery from manures coupled with reduction of waste volume, removal of organic contaminants and pathogens (Cao et al., 2019; Huang et al., 2018).

Hydrothermal carbonization (HTC) is one of the emerging thermochemical technologies used to upgrade solid fuel properties of the biomass due to its environmentally friendly and cost-effective pre-treatment method (Gascó et al., 2018; Lang et al., 2018). It involves the use of water as a reaction medium and mild temperatures (180 – 250 °C) to treat biomass under self-generated pressure (Dai et al., 2017). Thus, HTC has attracted particular attention for the treatment of livestock manures as pre-drying of biomass is

needless (Lang et al., 2019b). The product obtained from HTC is a slurry that can be efficiently dewatered by mechanical compression to obtain a hydrophobic hydrochar (HC) (moisture content: 20 – 50 %) with added value as a lignite-alike coal for combustion (Reza et al., 2015; Wang et al., 2014). The majority of studies on manure HTC have seemingly focused on investigating the influence of operating conditions on either the process itself or HC properties. In general, increasing HTC temperature improves solid-fuel properties of the HC (e.g., higher calorific value, fuel ratio, and lower H/C and O/C atomic ratio), while the energy yield is significantly reduced ascribing to the decreased hydrochar yield (Gao et al., 2018; Ghanim et al., 2016). Recently, (Cárdenas-Aguiar et al., 2019; Lang et al., 2018) have evaluated the combustion properties of HC derived from manure HTC by thermogravimetric analysis (TGA).

Additionally, the dewatering of HTC slurry produces a process water (PW), whose potential application has been overlooked to date. The PW obtained from manure HTC usually contains high organic matter content (chemical oxygen demand (COD): 7.7 – 13.4 g L^{-1}) due to the significant content of hydrocarbons with high molecular weight (e.g, aldehydes, phenols, ketones, furan, acids, nitrogen-containing species, and others) (Gao et al., 2018; Wu et al., 2017). Furthermore, the PW includes significant content of total Kjeldahl nitrogen (TKN: 0.8 – 1.4 g L^{-1}), phosphate (0.2 – 0.8 g L^{-1}), and heavy metals (e.g., Zn, Pb, Cr, and Cd) exceeding standard-limits for direct utilization on agricultural land (Xiong et al., 2019). Based on the aforementioned characteristics, the PW can be either valorized via AD or resource recovery. AD has been able to remove more than 50 % of the COD in the PW derived from HTC of sewage sludge (Villamil et al., 2020), microalgal biomass (Marin-Batista et al., 2019), and digestate (Aragón-Briceño et al., 2017). This technology usually allows complete removal of furans and partial elimination

of phenols from PW, although methane yields are generally affected by the presence of nitrogen-containing species (De la Rubia et al., 2018b; Villamil et al., 2019).

This work evaluates the potential of hydrothermal carbonization to valorize dairy manure into valuable materials for energy recovery. The suggested valorization route implies two stages. Firstly, we study the combustion characteristics of hydrochars as solid-fuel by TGA (comprehensive combustion index, ignition and burnt-out temperatures), which are quite useful to understand the kinetic of solids-fuel combustion and design combustion equipment at industrial scale (Jain and Sharma, 2011). Then, we analyze the anaerobic digestion of the PW (organic matter removal, presence of refractory compounds, kinetic of methane production), and estimate the energy recovery by coupling both combustion of hydrochars and anaerobic digestion of PW.

2. Material and Methods

2.1 Hydrothermal carbonization

Dry dairy manure was supplied from University of Nevada Reno (UNR) Main Station Farm (Reno, NV, USA). A typical manure collection and storage procedure involved scooping manure into plastic bags from a pile of fresh manure in the steer pen (Toufiq Reza et al., 2018). After collection, the manure was dried at open air condition for several days before being ground in a hammer mill (brand) to reduce the particle size in the range 0.5 – 3 mm. The dry dairy manure (936.3 ± 0.1 g kg^{-1} of total solids (TS), 758.5 ± 0.3 g kg^{-1} of volatile solids (VS)) was stored in a Ziploc bags.

Prior HTC experiments, dry dairy manure was rehydrated (1 to 10 mass ratio of dry manure to water) and characterized (165 ± 1.2 g kg^{-1} of TS, 152.7 ± 6.1 g kg^{-1} of VS,

148.1 ± 6.9 g O_2 kg^{-1} of total COD (TCOD)). The HTC tests were performed in an electrically heated 4 L ZipperClave® pressure vessel with a load of 2 kg of rehydrated dairy manure. Operating temperatures of 170, 200, and 230 °C were reached at a heating rate of 3 °C min^{-1} and then held for 1 h. The reaction was quenched by cooling with an internal heat exchanger using tap water. The slurry obtained at each HTC temperature was dewatered by vacuum filtration (0.90 μm). Then, the respective PW were filtered (0.45 μm), labelled as PW170, PW200 and PW230, related to the HTC temperature used, and stored (4 °C) for further use as substrate in AD tests. The hydrochars obtained were labelled as HC170, HC200, and HC230, related to the HTC temperature used, as well. The hydrochars were oven-dried overnight at 105 °C, and then ground and sieved. A Filter No. 38373 sieve was used to separate the hydrochars. The fraction with particle size lower to 0.25 mm was used for characterization purposes.

2.2 Thermogravimetric analysis

The combustion experiments were carried out under atmospheric pressure using a thermogravimetric analyzer (TG 209, F3, Netzsch, Germany). The experiment conditions were defined based on the non-isothermal combustion procedures reported by Cárdenas-Aguiar et al. (2019) and Lang et al. (2019a). 10 g of sample (dry manure, HC170, HC200, and HC230 with particle size lower than 0.25 mm), placed in an Al_2O_3 crucible, was heated from 50 to 900 °C at a heating rate of 10 °C min^{-1}. The carrier gas used was high purity air with a flow rate of 120 mL min^{-1}. The thermogravimetric (TG) experiment was repeated at least twice for each sample to ensure accuracy. The TG and differential TG (DTG) data provided the characteristic combustion parameters including ignition temperature (T_i), burnout temperature (T_b), maximum weight loss rate (DTG_m) and corresponding temperature (T_m) to evaluate the combustion behavior of each sample

(Zhou et al., 2019). Specifically, T_i indicates the temperature at which the fuel starts to burn, and T_b denotes the temperature for the complete combustion of fuel, and they are determined by the TG-DTG tangent method (Ma et al., 2006). T_m is defined as the temperature at which the weight loss rate reaches the maximum. Additionally, the comprehensive combustion index (CCI) is calculated using equation 1 (Lang et al., 2019a):

$$CCI\ (min^{-2}\ °C^{-3}) = \frac{DTG_m \cdot DTG_{mean}}{T_i^2 \cdot T_b} \quad (1)$$

where, DTG_m and DTG_{mean} indicate the maximum and average weight loss rate, respectively.

The first-order Doyle approximation (Eq. 2) is the most frequent assumed model to describe the kinetics of volatilization and decomposition reaction during hydrochar combustion (Lang et al., 2019a; Zhou et al., 2019):

$$ln\left[\frac{-ln\ (1-\alpha)}{T^2}\right] = ln\left[\frac{A \cdot R}{\beta \cdot E}\left(1 - \frac{2 \cdot R \cdot T}{E}\right)\right] - \left(\frac{E}{R}\right) \cdot \frac{1}{T} \quad (2)$$

where, E is the activation energy (kJ mol^{-1}); A is the pre exponential factor (min^{-1}); R is the universal gas constant (8.314 J K^{-1} mol^{-1}); T is the absolute temperature (K); α and β are the mass conversion fraction and heating rate, respectively (Lang et al., 2019a). If hydrochar combustion follows a first-order reaction mechanism, the plot of $\frac{-ln\ (1-\alpha)}{T^2}$ against $\frac{1}{T}$ will be a straight line. The activation energy (E) can be obtained from the slope, while the pre-exponential factor (A) is calculated from the intercept of this straight line (Zhou et al., 2019).

2.3 Anaerobic digestion experiments

AD runs of dry manure and PWs were carried out batch wise in 120 mL glass serum vials. The initial inoculum concentration was set at 15 g VS L^{-1} and the inoculum-to-substrate ratio (ISR) at 2 on a VS basis. The inoculum used was a granular anaerobic sludge from an industrial digester processing brewery wastewater under mesophilic conditions (35 °C). The inoculum showed the following characteristics: pH 7.2 ± 0.2; 80.7 ± 2.1 g TS L^{-1}; 70.9 ± 1.5 g VS L^{-1} and 70.7 ± 1.7 g O_2 L^{-1} of TCOD. A basal medium containing macro- and micronutrients prepared and dosed as described elsewhere (Villamil et al., 2018) was added, after which the reaction volume was made up to 60 mL with deionized water. The vials were sealed with rubber stoppers and metallic crimps and then the unfilled space of the vial (60 mL) was purged with N_2 for 3 min to ensure anaerobic conditions. Finally, the vials were held in a thermostatic shaking water bath at 80 rpm equivalent stirring and mesophilic temperature (35 ± 1 °C).

The time course of AD was followed by using ten vials for each of the PW samples obtained at the three HTC temperatures tested (PW170, PW200, PW230) and for the rehydrated manure. Seven of them were sacrificed: two during the first three days and then every week. The remaining three vials were used for biogas analysis (volume and composition) only. Triplicate blank samples containing no substrate were also used to establish the background biogas level from the inoculum. Specific methane yield (SMP) was calculated by subtracting the amount of methane produced by the blanks from the amount of methane production exceeding the initial VS added value for each substrate in each batch reactor.

2.4 Calculations

196 The calculation of energy output was made based on the HHV of hydrochar and process
197 water. The mass yields of hydrochar (Y_{HC}) and process water (Y_{PW}) on a TS basis were
198 defined as the respective weight ratio of recovered HTC product (HC or PW, $W_{HC,\,PW}$) to
199 feedstock (W_F) fed into the HTC reactor, equation (3):

$$Y_{HC,PW}\ (\%) = \left(\frac{W_{HC,PW}}{W_F}\right) \cdot 100 \qquad (3)$$

200 The values of *SMY* obtained in the AD tests were used to calculate the HHV of process
201 water (HHV_{PW}), based on equation (4):

$$HHV_{PW}(MJ\ kg^{-1}) = 39.8 \cdot SMY \cdot \left(\frac{VS}{TS}\right) \qquad (4)$$

202 where, the *VS to TS ratio* corresponds to the substrate added into the anaerobic reactor,
203 and *39.8* is the HHV of pure methane in MJ Nm^{-3}.
204
205 The total energy associated to HTC products was calculated by equation (5):

$$\text{Energy recovery}\left(\text{MJ kg}^{-1}{}_{\text{feedstock}}\right) = \text{HHV}_{\text{HC}} \cdot \text{Y}_{\text{HC}} + \text{HHV}_{\text{PW}} \cdot \text{Y}_{\text{PW}} \qquad (5)$$

206 where, HHV_{HC} corresponds to HHV (MJ kg^{-1}) of hydrochars.
207
208 **2.5 Analytical methods**
209 The dried solid samples (manure and hydrochars) were analyzed by elemental
210 composition determined with a CHNS analyzer (LECO CHNS-932, Model 601-800-
211 500), using the manufacturer's standard procedures. Proximate analysis (ash, fixed
212 carbon (FC), and volatile matter (VM) was done by TGA according to American society
213 for testing and materials (ASTM; D7582 (ASTM, 2015)). The HHV of solid samples
214 were determined by using an IKA C2000 bomb calorimeter according to technical
215 specification EN 15400 (EN 15400:2011, 2011). Major elements in ashes were analyzed
216 by ICP-MS with an Elan 6000 Sciex instrument (Perkin Elmer).

The rehydrated manure, process waters and the inoculum were characterized by measuring pH with a Crison 20 Basic pH-meter; TS and VS according to standard method 2540B and 2540E, respectively (APHA, 2005) and total organic carbon (TOC) in a Shimadzu TOC–VCPN auto analyzer. TKN was determined as described elsewhere (Villamil et al., 2018) and the TCOD according to Raposo et al. (2008). PWs and sacrificed samples from the AD tests (centrifuged and filtered through a filter of 0.45 μm pore size) were analyzed as follows: Soluble COD (SCOD) according to standard method 5220D (APHA, 2005); carbohydrates by colorimetric method (Dubois et al., 1956); proteins with the Folin phenol method (Randall and Lewis, 1951); total alkalinity (TA) by titration to pH 4.3 with 0.02 N H_2SO_4 and total ammonia nitrogen (TAN) by distillation and titration according to standard methods 2320B and 4500-NH_3, respectively (APHA, 2005). The concentrations of individual volatile fatty acids (VFAs) from acetic to heptanoic, iso-forms included, were determined by gas chromatography (GC) in a Varian 430-GC instrument equipped with a flame ionization detector (FID) and a capillary column filled with Nukol (nitroterephthalic acid-modified polyethylene glycol) (De la Rubia et al., 2018b). Chemical species were identified in a GC–MS CP-3800/Saturn 2200 instrument equipped with a Varian CP-8200 auto sampler injector (De la Rubia et al., 2018a). Compounds were identified against the NIST 2008 Library. Biogas production was assessed manometrically (Villamil et al., 2018) by measuring the pressure increase in each vial with an electronic pressure monitor (ifm, PN7097). The amount of biogas was expressed under standard temperature and pressure conditions (STP; 273 K and 1 bar). Finally, the gas composition (H_2, CO_2, and CH_4) was determined on a Thermo Scientific Trace 177 1310 GC (De la Rubia et al., 2018a).

3. Results

3.1 Hydrochar as solid fuel

A representative analysis of dairy manure and hydrochars is shown in Table 1.

Table 1. Characteristics of dairy manure and hydrochars[a] (dry basis).

	Dairy Manure	HC170	HC200	HC230
HC mass yield (%)	-	65.0	57.0	54.0
FC (%)	15.7	12.5	17.0	18.7
VM (%)	68.8	67.8	59.7	57.2
Ash (%)	15.5	19.7	23.3	24.1
C (%)	39.9	41.6	44.8	47.4
H (%)	5.3	5.3	5.3	5.3
N (%)	2.7	2.0	2.1	2.1
S (%)	0.5	0.2	0.1	0.1
O (%)[b]	36.1	31.2	24.4	21.0
HHV (MJ kg^{-1})	16.0	16.4	19.0	20.1
Fuel ratio	0.23	0.19	0.23	0.33
T_i (°C)	252	263	270	278
T_b (°C)	573	581	601	619
T_m (°C)	308	316	320	315
DTG_m (% min^{-1})	5.6	7.0	4.8	3.9
$CCI \cdot 10^7$ (min^{-2} $°C^{-3}$)	1.4	1.6	0.9	0.7
$E_{devolatilization}$ (kJ mol^{-1})	21.5	32.2	31.3	26.6
$E_{combustion}$ (kJ mol^{-1})	42.9	23.0	22.2	22.5

[a] Each data showed a standard deviation ≤ 0.3
[b] By difference

After HTC, the carbon content of hydrochars increased gradually while the oxygen content decreased considerably with the increase of temperature. These changes could be explained by means of van Krevelen diagram (Fig. 1). The evolution of the H/C and O/C ratios during HTC followed the progression of dehydration and decarboxylation reactions, while the demethanation pathway was negligible. Seemingly, the trends of dehydration and decarboxylation became increasingly apparent at higher HTC temperatures due to increase in reaction rates (Zhang et al., 2018). Thus, HC230 reached H/C and O/C atomic ratios comparable to those in lignite, while HC170 and HC200 showed H/C and O/C atomic ratios comparable to those in peat. Nitrogen and sulphur

contents of hydrochars were lower than those of the feedstock (dairy manure), as previously found for swine manure (Gascó et al., 2019) and poultry manure (Ghanim et al., 2016), which may result in scant formation of SO_x and NO_x species through hydrochar combustion (Cárdenas-Aguiar et al., 2019; Liu et al., 2019).

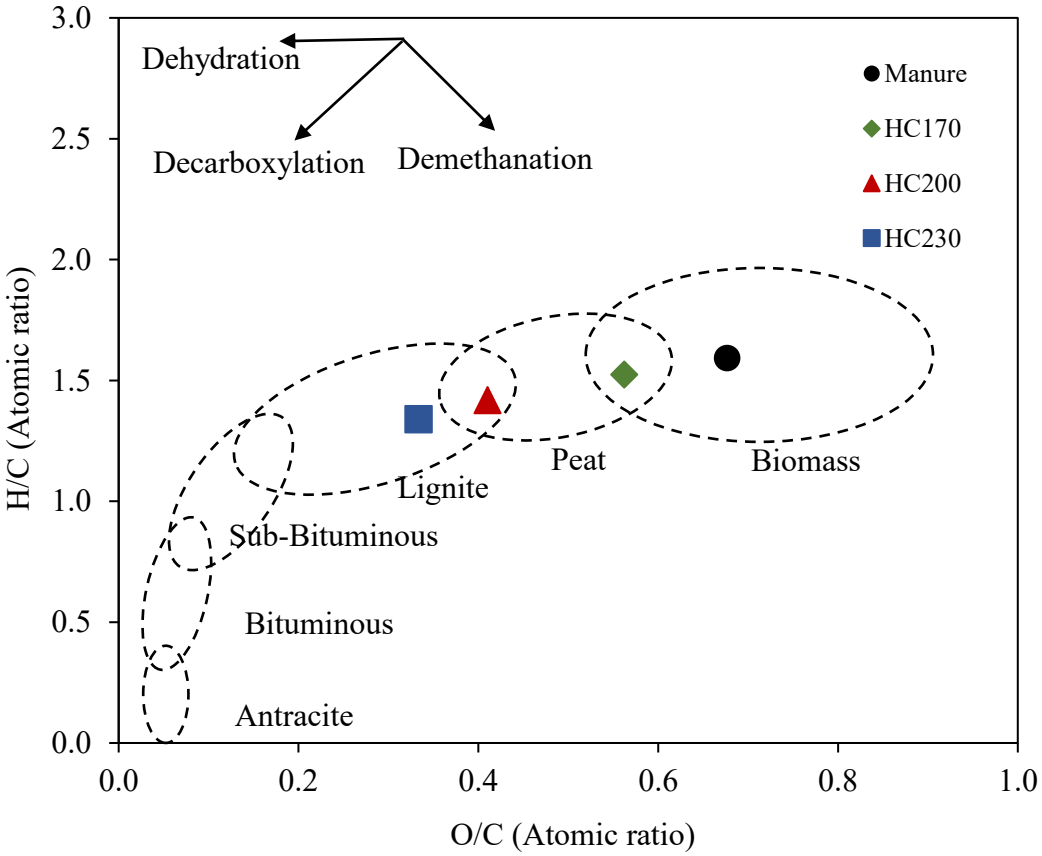

Fig. 1. van Krevelen diagram for dairy manure and hydrochars upon HTC of dairy manure at 170, 200, and 230 ºC

On the other hand, the increase in HTC temperature affected the fuel ratio (FC/VM), which has been used to rank hydrochars as effective alternative coal based fuels (Marin-Batista et al., 2019). Thus, fuel ratio increased gradually from 0.19 to 0.33, ascribing to increase in FC content and a rising trend of VM loss with increasing HTC temperature. Increase in fuel ratio can be considered positive due to higher FC content in HCs, which

in turn improved HHV from 16.0 (feedstock) to 20.1 (HC230) MJ kg^{-1}. Nevertheless, increasing HTC temperature also led to excessive VM loss from the feedstock, giving rise to ash content in HCs from 19.7 (HC170) to 24.1 % (HC230). In the meantime, the hydrochar energy yield (HHV multiplied by HC mass yield) did not vary with increase in HTC temperature (around 10 MJ kg^{-1} feedstock for each HTC condition), due to the decrease in hydrochar yield.

Fig. 2 shows the TG and DTG analysis. From the DTG curves, an initial mass loss was observed for each solid-fuel between 50 and 180 °C, corresponding to loss of moisture and very light VM (Liu et al., 2019). Thereafter, two major DTG-picks were found for all the samples. The first DTG-pick, located around 315 ºC, represents a devolatilization period for light compounds and carbohydrates such as cellulose or hemicellulose (Cárdenas-Aguiar et al., 2019). While, the second DTG-pick, located between 410 and 500 ºC, is attributed to decomposition/combustion of more stable structures with high molecular weight such as lignin in conjunction with combustion of FC (Niu et al., 2016). HTC temperature remarkably influenced the combustion behavior of each hydrochar. The length of the first DTG-pick decreased with increase in carbonization temperature, while the width (combustion temperature range) of the second-pick increased for each hydrochar. These observations are in accordance with the results reported by Lang et al. (2019a), and it is most likely due to increase in fuel-ratio (decreased VM and increased FC content) to more sever HTC temperature (see Table 1).

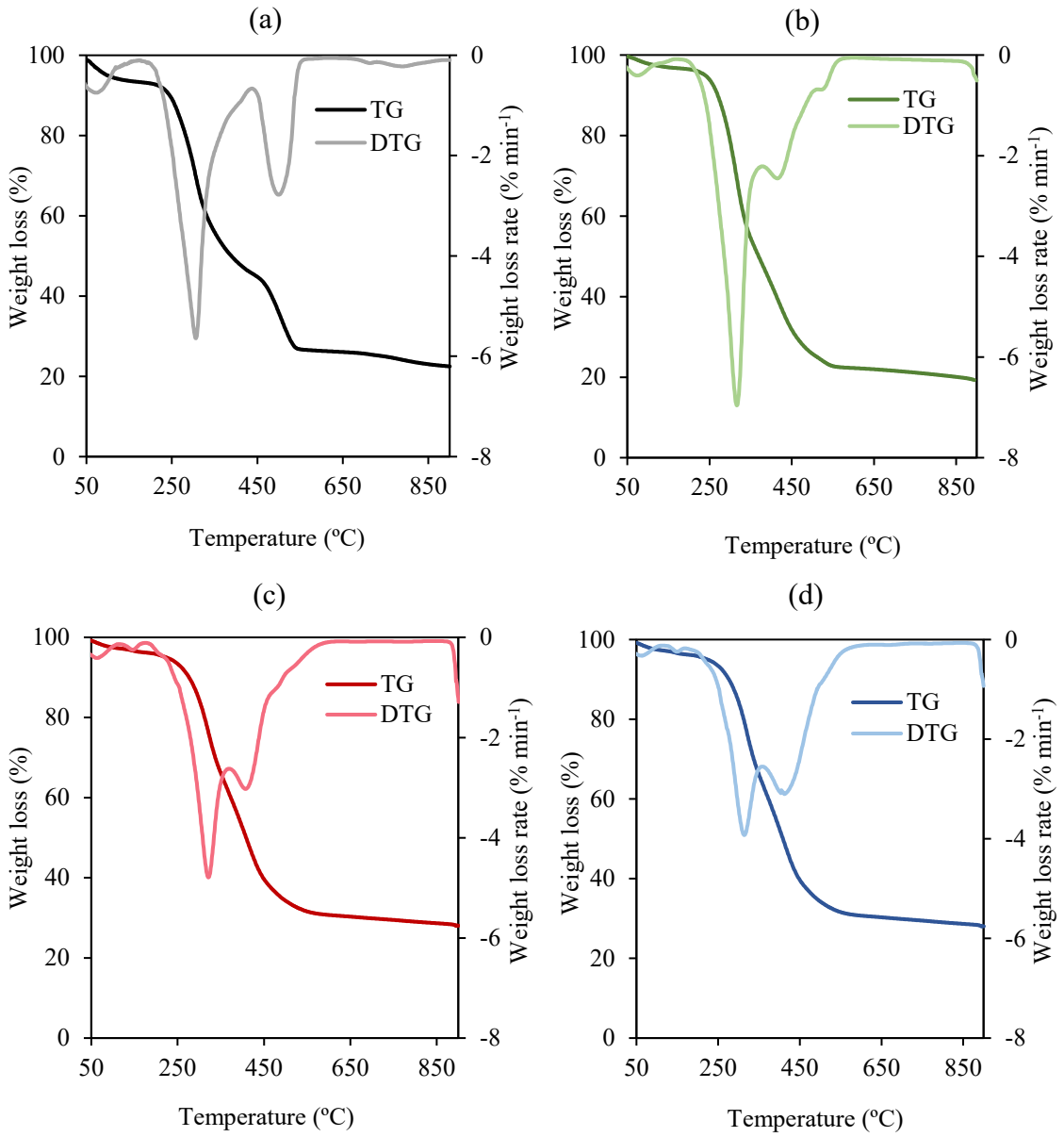

Fig 2. TG and DTG profiles of dairy manure (a), HC170 (b), HC200 (c), HC230 (d).

Table 1 also shows the combustion parameters of dry dairy manure and hydrochars. Increase in HTC temperature resulted in significant changes of the characteristic combustion parameters. The T_i and T_b increased gradually along with the carbonization temperature. Therefore, converting dairy manure into hydrochar would increase the ignition difficulty and thus reduced the risk of fire and explosion (Zhou et al., 2019). However, higher burnout temperatures implied larger retention times in a continuous combustion process, which is inconvenient considering the large content of ash in

hydrochar (Ahn et al., 2020). Thus, HC170 showed the best combustion performance as CCI and R_w of HC200 and HC230 were much lower than those of HC170 and even the raw biomass, implying that the combustion properties of HC200 and HC230 were inferior.

There were significant differences in the activation energy of devolatilization and decomposition/combustion stages between raw manure and hydrochars. The activation energy of hydrochars at devolatilization stage were higher than that of raw manure and vice versa at decomposition/combustion stage (Table 1). The higher activation energy of hydrochar at devolatilization stage might be caused by the high degree of carbonation, which can be seen in the van Krevelen diagram (Fig.1). Additionally, some specific properties of hydrochar, such as surface area, surface functionalities, and porosity, usually show higher values than those of raw manure (Zhou et al., 2019). Likewise, the high content of inorganic species in hydrochar (Table 2) may have a catalytic effect on the thermal degradation of lignin and fixed carbon, which could lead to lower activation energy at decomposition/combustion stage.

On the other hand, the ash chemistry can hinder the combustion of hydrochar. Having a high ash melting temperature is often desirable, as most furnaces are designed to remove ash as a powdery residue. Otherwise it has a higher tendency to fuse into a hard glassy slag, known as a clinker, which leads to heat transfer bottlenecks usually solved by halting the furnace operation to allow cleaning (Smith et al., 2018). Alkali metals, potassium, and sodium generally reduce the ash melting temperature, while earth metals magnesium and calcium commonly increase it. In other words, a low-alkali-metal content within hydrochar is desirable to avoid ash slagging and fouling issues (Smith et al., 2016). Table

2 shows the major ash forming elements in dairy manure and HCs. Increase in HTC temperature significantly decreased the content of K and Na in hydrochar, while Mg and Ca showed negligible variation. Smith et al. (2016) studied the influence of HTC on the ash melting-point of different biomass (e.g., oak wood, greenhouse waste, food waste, digestate, sewage sludge, microalgae), confirming that removal of K and Na has a strong influence on the slagging propensity of the fuel, with ash fusion temperatures for hydrochar melting at higher temperatures to that of the raw feedstock. For instance, microalgae ash melting-point of 660 ºC was significantly increased up to 970 and 1180 ºC when HTC was conducted at 200 and 250 ºC.

Table 2. Major elements in the ash fraction of dairy manure and hydrochars (dry basis)

	Dairy manure	HC170	HC200	HC230
K	0.91	0.25	0.10	0.15
Na	0.44	0.17	0.10	0.14
Mg	0.50	0.48	0.42	0.43
Ca	2.82	2.75	2.78	2.75
P	0.25	0.26	0.27	0.34

Note: (wt. %). Each data showed a standard deviation ≤ 0.05

Conversely, the rising trend of P content in hydrochars suggests that HTC facilitates P immobilization in dairy manure. Dai et al. (2015) showed that organic P in dairy manure reacts with multivalent metal elements (i.e., Ca, Fe, Mg and Al) during HTC, increasing the amount of inorganic phosphate salts in hydrochars. Therefore, P in dairy manure after thermal treatment is much less soluble than that in untreated biomass and hence HTC can potentially alleviate manure issues related to eutrophication of ground water sources due to P loss during long-term storage (Huang et al., 2018).

3.2 Mesophilic anaerobic digestion of process water

The characteristics of the PWs obtained by HTC of dairy manure are collected in Table 3.

352 Table 3. Representative analysis of process water.

	PW170	PW200	PW230
TS (g L^{-1})	19.2 (0.1)	28.4 (0.4)	24.1 (0.9)
VS (g L^{-1})	14.2 (0.1)	20.3 (0.3)	16.2 (0.8)
SCOD (g O_2 L^{-1})	12.8 (0.6)	18.3 (0.9)	21.3 (0.5)
TOC (g L^{-1})	6.61 (0.1)	10.9 (0.1)	10.7 (0.1)
TKN (g N L^{-1})	2.4 (0.6)	3.5 (0.1)	4.9 (0.2)
pH	6.9 (0.1)	6.3 (0.1)	5.9 (0.1)
Total alkalinity (g $CaCO_3$ L^{-1})	1.2 (0.1)	1.5 (0.1)	1.5 (0.3)
N-NH_3 (g N L^{-1})	0.3 (0.1)	0.7 (0.1)	0.9 (0.1)
VFA (g COD L^{-1})	2.9 (0.2)	2.5 (0.1)	2.4 (0.1)

Note: Standard deviation in parentheses

353 During the HTC process, macromolecular organic matters (e.g., cellulose, hemicellulose,
354 polymers, long chain fatty acids, proteins, etc.) in feedstock would gradually hydrolyze
355 into soluble organic matter (e.g., sugars, amino acids, VFA, phenols, alcohols, etc.) with
356 increasing reaction temperature (Gao et al., 2018). Thus, SCOD and TOC showed an
357 upwards trend by increasing the temperature from 170 to 230 ºC. Particularly, proteins
358 are hydrolyzed to peptides and amino acids, which in turn are oxidatively degraded to
359 fatty acids and ammonia (Chen et al., 2019). Significantly high content of TKN were
360 found in PW170 and increased with increase in the HTC temperature. The same trend
361 was observed for ammonia and TA. By the contrary, total VFA (TVFA) concentration of
362 PW decreased with increase in the HTC temperature, which might be due to the
363 degradation of soluble organic compounds at severer HTC temperature (Xiong et al.,
364 2019).

365

366 During AD, methanogenic microorganisms use VFA for methane production. Thus, the
367 time course of individual VFA (Fig. 3) provides useful information on the performance
368 of the acidogenesis and methanogenesis stages in AD.

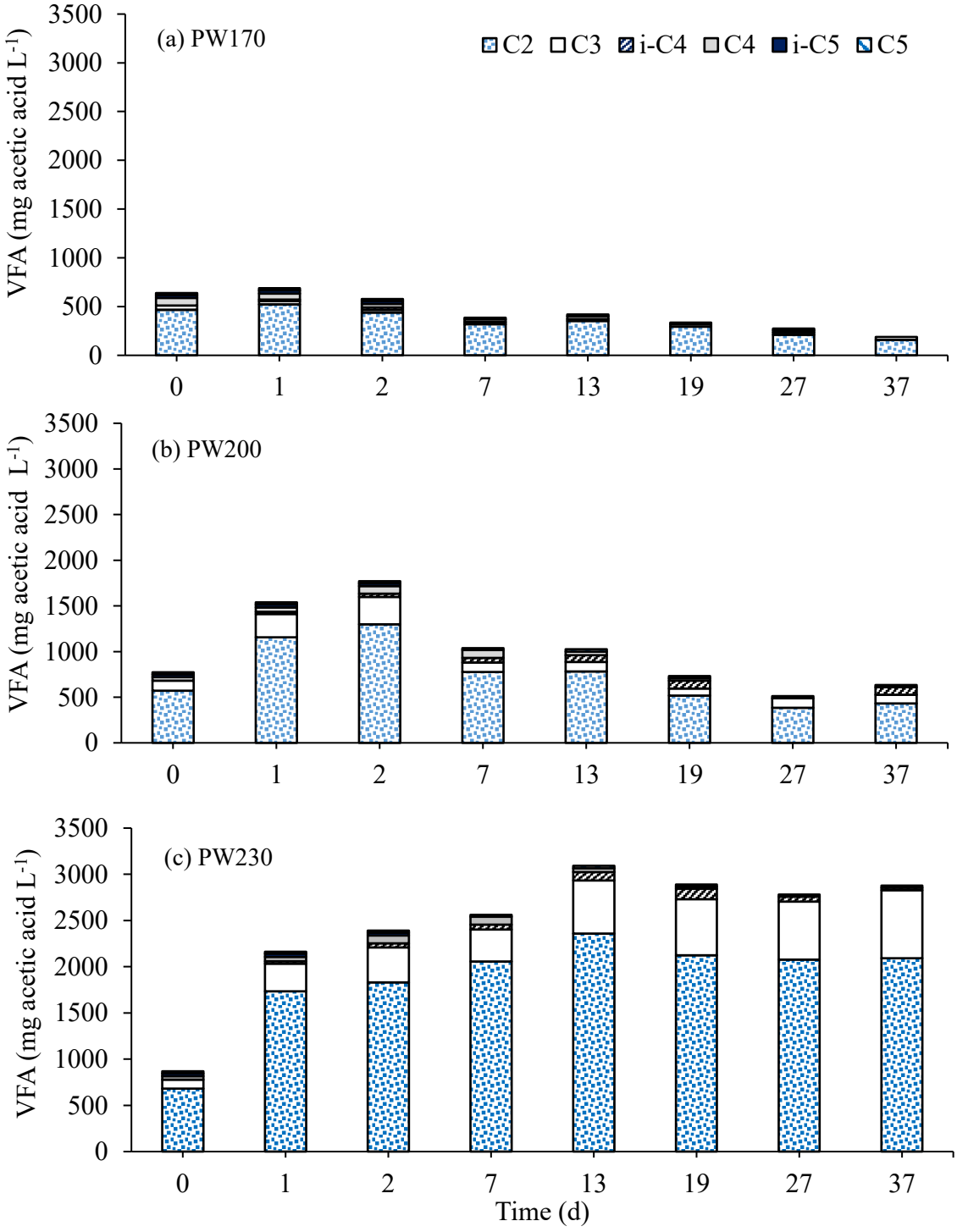

369
370
371

372 Fig. 3. Time course of the relative distribution of individual components of the total
373 volatile fatty acids fraction (expressed as acetic acid concentration) upon AD of PWs.

374 Acetic acid (C2) was the major VFA present at the beginning of the experiment,
375 accounting for around 70 – 80 % of TVFA. While, longer chain VFAs such as valeric
376 (C5) and iso-valeric (i-C5) as well as butyric (C4) and iso-butyric (i-C4) were present in
377 low concentrations (< 50 and < 100 expressed as mg of acetic acid L^{-1}, respectively). The
378 concentration of longer chain VFAs gradually decreased during the first couple days of
379 AD due to the effective acetogenic stage, wherein VFAs are mainly converted into C2
380 and C3. Thus, the concentration of TVFA expressed as mg of acetic L^{-1} increased rapidly
381 for PW170 (up to 1800 mg of acetic L^{-1}) and PW170 (700 mg of acetic L^{-1}) and afterwards
382 decreased gradually due to the formation of methane from acetate. At the end of the
383 experiment, the TVFA concentration for PW170 (189 ± 6 mg equivalent of acetic L^{-1})
384 and PW210 (632 ± 9 mg equivalent of acetic L^{-1}) accounted for TVFA reduction of 73
385 and 65 %, respectively. This notable reduction of the VFAs concentration demonstrates
386 that the methanogenic stage was not disturbed for the PW170 and PW200. In contrast,
387 TVFA accumulated in PW230 run, reaching concentrations of 3314 and 2950 mg
388 equivalent of acetic per liter at day 13^{th} and at the end of the experiment, respectively,
389 which is the result of production and elimination reactions being uncoupled. In this
390 situation, methanogens are unable to remove volatile organic acids fast enough and
391 imbalances in biogas production result (Raposo et al., 2011).
392
393 The values of pH, TA, and TAN are normally closed related. For all runs, the pH varied
394 within the range of 7.0 to 8.3, adequate level for the growth of methanogens (De la Rubia
395 et al., 2018a). The TA was initially below 1.1 g L^{-1} $CaCO_3$ for all the runs and increased
396 above 2 g L^{-1}, providing enough buffer capacity to cope with changes in pH. Increase in
397 TA during AD is commonly related to the effective conversion of TKN into TAN
398 (Villamil et al., 2020). For all the runs, the initial TAN concentrations ranged from 0.2 to

399 0.5 g N L^{-1}, reaching 1.7 g N L^{-1} (for the PW170) and 1.9 g N L^{-1} (PW200), at the end of
400 the experiment, which are below to TAN inhibitory concentration (≈ 2000 mg N L^{-1}) (De
401 la Rubia et al., 2018b). In the meantime, PW230 reached TAN concentration of 2.3 g N
402 L^{-1}, slightly higher than the aforementioned inhibitory value that could potentially
403 inhibited VFA uptake during methanogenic stage.
404
405 Fig. 4 shows the cumulative methane yield produced during the AD of rehydrated dairy
406 manure and process water. The methane production immediately started and progressed
407 exponentially throughout the AD. The final methane yields obtained were 294 ± 2, 235 ±
408 8, and 80 ± 4 mL STP CH_4 g^{-1} VS_{added} for PW170, PW200 and PW230, respectively.
409 Notably, the cumulative methane yield showed a downward trend by increase in HTC
410 temperature, which was in accordance with the trends of SCOD removal upon AD (49.1
411 and 38.4 % for PW170 and PW200, respectively). This fact was much more significant
412 for PW230, which showed an accumulation of SCOD consistently with the accumulation
413 of VFA. The non-biodegraded SCOD can be assigned to refractory compounds formed
414 during HTC of dairy manure, whose concentration significantly increases to severer HTC
415 temperature (Gao et al., 2018; Wu et al., 2017).

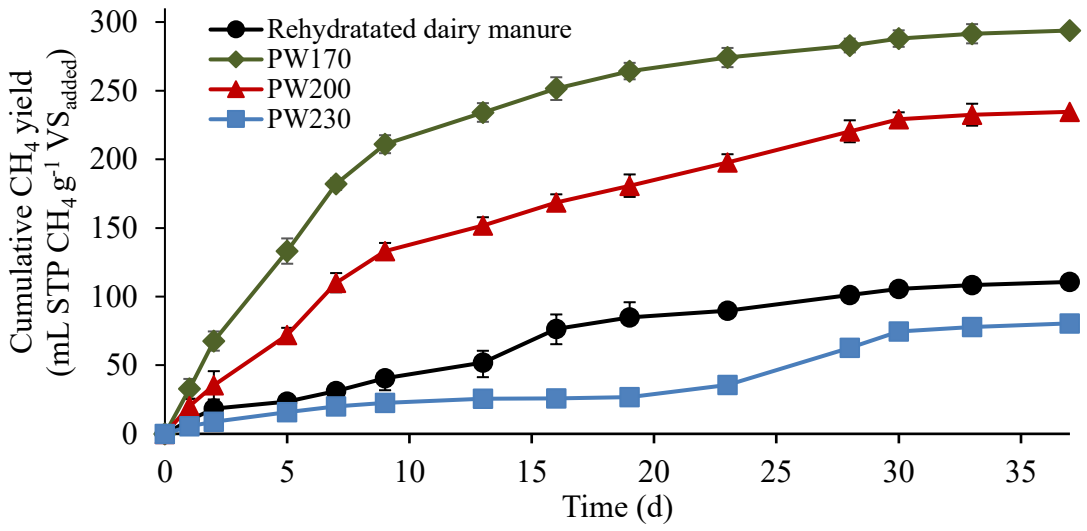

416

417 Fig. 4. Cumulative methane yield along the anaerobic digestion of PW.

418

419 The PW170 and PW200 exhibited greater methane yields than that for rehydrated dairy
420 manure (110 ± 2 mL STP CH_4 g^{-1} VS_{added}) and that typically reported for fresh dairy
421 manure under mesophilic conditions, ranging from 176 to 220 mL STP CH_4 g^{-1} VS_{added}
422 (Imeni et al., 2019; Passos et al., 2017). Thus, the valorization of PW via AD is of high
423 interest, as it contributes with additional energy recovery in form of biogas. The
424 cumulative CH_4 yields were modelled using the first-order kinetic equation, Gompertz
425 model, and Cone equation, which are widely used for AD (Raposo et al., 2011; Villamil
426 et al., 2019; Zhao et al., 2016). Table 4 collects the kinetic equations applied to fit the
427 experimental results using curve fitting (cftool) toolbox from Matlab R2105a (Licence
428 No. 40653209).

429

430 Table 4. Kinetic model used to fit the experimental results of cumulative methane yield.

Model	Equation	Parameter
First-order	$\boldsymbol{G(t) = G_{max} \cdot [1 - exp\,(-k \cdot t)]}$	G (mL CH_4 g^{-1} VS): cumulative CH_4 yield
Gompertz	$\boldsymbol{G(t) = G_{max} \cdot exp\,[-exp\,(\mu - \lambda \cdot t)]}$	G_{max} (mL CH_4 g^{-1} VS): ultimate CH_4 yield
Cone	$\boldsymbol{G(t) = \frac{G_{max}}{1 + (k \cdot t)^{-n}}}$	k (d^{-1}): specific rate constant t (d): digestion time μ (mL CH_4 g^{-1} VS d): maximum

431

432 Table 5 summarizes the experimental CH_4 yields and fitting parameters. The kinetics
433 models provided accurate prediction of the experimental data with determination
434 coefficients (R^2) > 0.978, except for PW230 (data not shown). Because the proposed
435 kinetics models fail to represent complex degradation pattern as occurred with PW230

436 run. This adopts a CH_4 production as stepped curve which is typical for degradation of
437 complex and/or the production of inhibitory intermediate products (Ware and Power,
438 2017). The maximum CH_4 yield was best fitted to Gompertz model with errors < 6 %.
439 The specific rate constant (*k*) varied from 0.039 – 0.130 d^{-1}. In this study, the highest
440 value was observed for the lowest carbonization condition (PW170), being improved by
441 33 and 76 % in comparison with dairy manure and PW200 runs. The lower *k* values
442 showed by PW200 hints mass transport limitation during AD (Zhao et al., 2016), thus
443 low HTC temperature are recommended to improve the valorization of dairy manure.
444
445 Table 5. Experimental maximum methane yield* (G_{me}) and fitting parameters of the
446 models checked for the anaerobic experiments

	Parameters	Manure	PW170	PW200
Experimental*	**Gme (mL CH_4 g^{-1}**	111 (20)	294 (12)	235 (21)
First-order	**Gm (mL CH_4 g^{-1}**	151 (14)	292 (3)	251 (6)
	k (d^{-1})	0.039	0.130	0.074
	R^2	0.985	0.998	0.994
Gompertz	**Gm (mL CH_4 g^{-1}**	117 (4)	282 (5)	230 (8)
	k (mL CH_4 g^{-1} VS	1.036	0.936	0.888
	λ (d)	0.109	0.236	0.142
	R^2	0.989	0.986	0.978
Cone	**Gm (mL CH_4 g^{-1}**	187 (50)	323 (6)	332 (30)
	k (d^{-1})	0.213	0.058	0.092
	n	1.160	1.269	1.031
	R^2	0.983	0.998	0.995

447 Note: Standard deviation in parentheses; p-value <0.05 for all parameters
448
449 Fig 5. shows a representative semi-quantitative analysis of the chemical compounds in
450 PW170, PW200 and PW230 before and after AD. The species have been clustered in
451 chemical groups and their concentrations are expressed in terms of GC peak area (%).
452 Raising the HTC temperature boosted the diversification of chemical species in the PW.

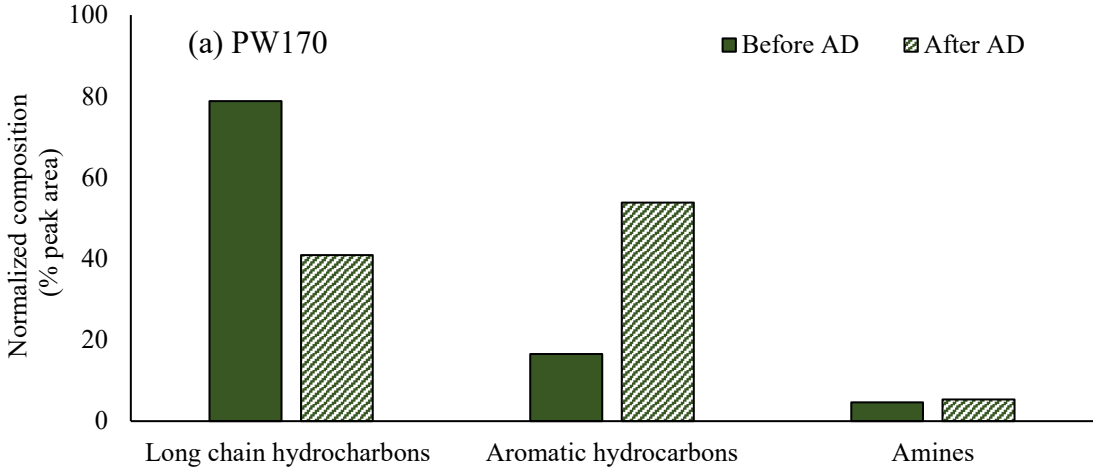

453

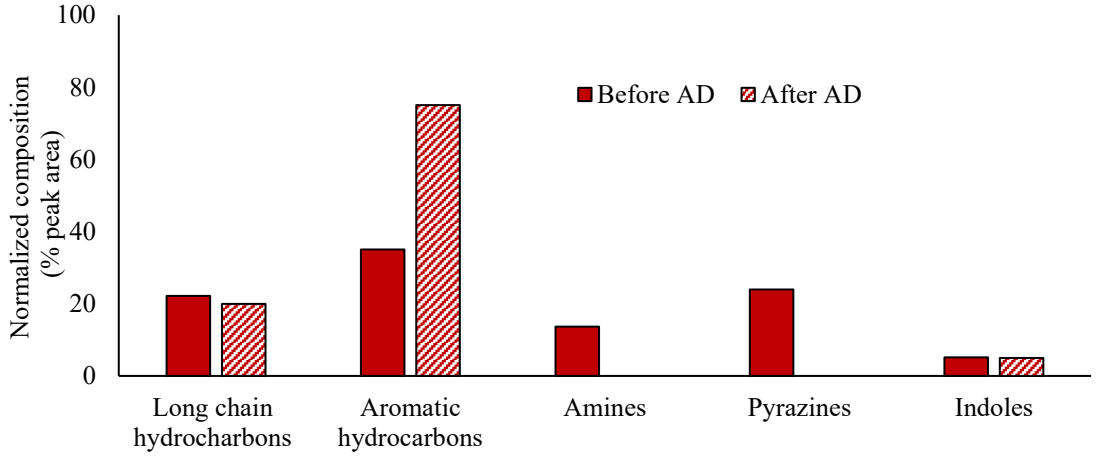

454

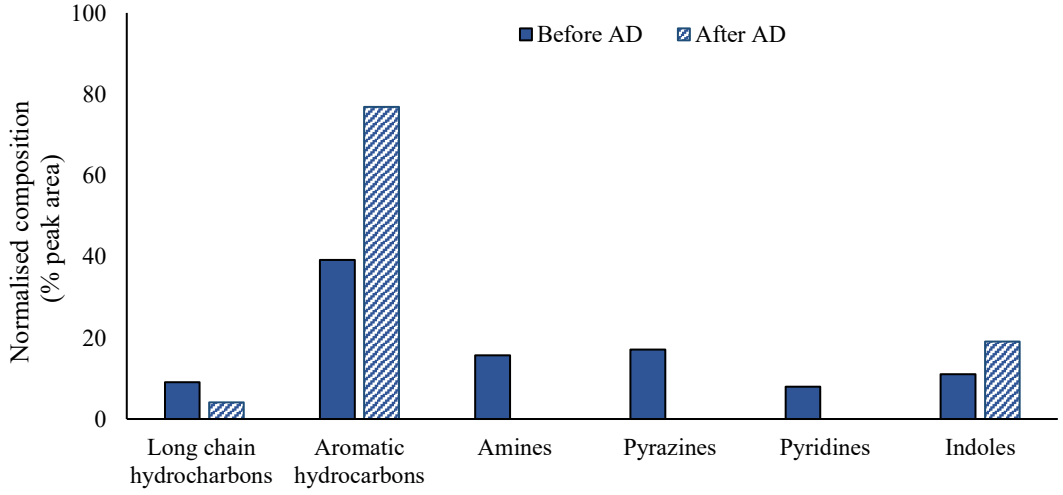

455

456 Fig. 5 GC/MS analysis of chemical species in PWs before (fulfill) and after (strings) AD

457

458 The PW170 showed significant content of long-chain hydrocarbons (e.g., 2-
459 trimethylsilyl-ethanol, undecanoic acid, tridecane) and aromatic hydrocarbons (e.g., 1,4-
460 benzenediamine, N-acetylcolchinol methyl ether), which were most likely produced due
461 to the thermal degradation of cellulose and hemicellulose fraction in the feedstock (Reza
462 et al., 2016). Increasing HTC temperature provoked significant reduction in the content
463 of some long-chain hydrocarbons (e.g undecanoic acid and tridecane), and appearance of
464 new aromatic hydrocarbons characteristic for HTC condition at 200 ºC (2,3,6-
465 trichlorobenzaldehyde) and 230 ºC (1,3,5-cycloheptatriene, ethylbenzene, 2-methoxy-
466 phenol, 4-hydroxy-benzenemethanol). After AD, some long-chain hydrocarbon (2-
467 trimethylsilyl-ethanol) identified in each PW were still present, indicating to be refractory
468 to anaerobic biodegradation. Additionally, new aromatic hydrocarbons were present at
469 the end of AD of PW200 (2,4,6-trimethoxyacetophenone) and PW230 (and 2,4,6-
470 trimethoxyacetophenone), accounting for above 70 % of normalized composition.
471
472 On the other hand, raising the HTC temperature expanded the diversity of nitrogenated
473 species in PW. The nitrogen containing species in PW170 were amines (e.g.,
474 penicillamine), formed mainly through hydrolysis of proteins (Chen et al., 2019).
475 Increasing the HTC temperature above 200 °C led to compounds with one or two N
476 heteroatoms (e.g., pyrroles, indoles, amines) being present in PWs alongside other
477 nitrogenated aromatic compounds formed in Maillard-type reactions such as pyrimidines
478 (e.g., 2-aminopyridine and 5-methyl-7-amino-s-triazolo-pyrimidine) and pyrazines (e.g.,
479 2-ethyl-5-methyl-pyrazine). Pyrazines and pyrimidines were completed removed by AD.
480 The presence of indoles at the end of AD experiments is a clearly indicator the process
481 inhibition occurred for PW230 as a result of poor digestion, as was reported for AD of

PW derived from sewage sludge (De la Rubia et al., 2018b) and microalgal biomass (Marin-Batista et al., 2019).

3.3 Net energy recovery

Table 6 shows the amount of energy produced per kg dry feedstock for the valorization of dairy manure by conventional AD and the HTC–AD combination. The energy recovery from dairy manure by conventional AD is limited owing to the low methane yield resulting from the also low degradability of the lignocellulosic organic fraction in dairy manure (Passos et al., 2017). Imeni et al. (2019) showed that the codigestion of dairy manure with cheese whey (mixing ratios of 70:30 wt.%) increased the energy recovered by 80 % in comparison with the sole digestion of dairy manure, which can potentially improve the profitability of AD in medium dairy farms. HTC provides an alternative valorization route for dairy manure by recovering energy through hydrochar and methane from AD of the PW.

The HHV for dairy manure obtained in this work, 16.0 MJ kg^{-1}, was considered as the total amount of energy stored in the feedstock (see Table 1). AD of dairy manure provided 4.1 MJ kg^{-1} dry feedstock, which corresponded to only 25.6 % of the net amount stored in feedstock. The combustion of hydrochar in conjunction with AD of PW obtained at HTC operational temperature of 170 and 200 °C, provided the largest amount of energy produced (~13.7 MJ kg^{-1} dry feedstock, which accounted for an energy recovery yield of ~85 %). By contrast, combustion of HC230 plus AD of PW230 provided 11.8 MJ kg^{-1} dry feedstock (viz., 73.8 % of the total energy stored in dairy manure), which is so much lower due to the negligible contribution of AD of PW230. Thus, HTC temperatures below 200 °C is recommended to improve the valorization of dairy manure by HTC–AD.

Table 6. Energy produced and net energy recovery for the valorization of dairy manure using conventional AD and HTC coupled with AD

	Energy recovered (MJ kg^{-1} feedstock)			Energy recovery yield (%)
	Combustion	AD	Total	
Dairy Manure	-	4.1	4.1	25.6
(HC+PW)170	10.6	3.0	13.6	85.0
(HC+PW)200	10.8	2.9	13.7	85.6
(HC+PW)230	10.8	1.0	11.8	73.8

4. Conclusion

This study suggests a novel valorization route for dairy manure by hydrothermal carbonization and anaerobic digestion. A mild temperature (170 – 200 ºC) is recommended for HTC of dairy manure in order to obtain hydrochars with attractive comprehensive combustion index and a process water with relatively low content of refractory compounds, yielding additional energy in form of biogas. HTC at 170 ºC led to an energy recovery (energy content of hydrochar and methane from anaerobic digestion of process water) around 85 % of the total energy content of feedstock, 3.3-fold higher than the obtained from the anaerobic digestion of rehydrated cow manure.

Acknowledgments

Authors greatly appreciate funding from Spain's MINECO (project PID2019-108445RB-I00; project RYC-2013-12549), Madrid Regional Government (project P2018/EMT-4344), and National Science Foundation (NSF#CBET-1856009). Authors thank to Instituto Colombiano de Crédito Educativo y Estudios Técnicos en el Exterior (Colombia) as part of the grant awarded to José D. Marin-Batista. The authors thank Miguel Domene for his valuable help.

528

529 **References**

530 Ahn, H., Kim, D., Lee, Y., 2020. Combustion characteristics of sewage sludge solid
531 fuels produced by drying and hydrothermal carbonization in a fluidized bed.
532 Renew. Energy 147, 957–968. https://doi.org/10.1016/j.renene.2019.09.057

533 APHA, 2005. Standard methods for the examination of water and wastewater. Am.
534 Public Heal. Assoc. Washington, DC, USA. https://doi.org/30M11/98

535 Aragón-Briceño, C., Ross, A.B., Camargo-Valero, M.A., 2017. Evaluation and
536 comparison of product yields and bio-methane potential in sewage digestate
537 following hydrothermal treatment. Appl. Energy 208, 1357–1369.
538 https://doi.org/10.1016/j.apenergy.2017.09.019

539 ASTM, 2015. Standard Test Methods for Proximate Analysis of Coal and Coke by
540 Macro Thermogravimetric Analysis. Method D7582-15. ASTM Int. Pennsylvania.

541 Cao, Z., Jung, D., Olszewski, M.P., Arauzo, P.J., Kruse, A., 2019. Hydrothermal
542 carbonization of biogas digestate : Effect of digestate origin and process
543 conditions. Waste Manag. 100, 138–150.
544 https://doi.org/10.1016/j.wasman.2019.09.009

545 Cárdenas-Aguiar, E., Gascó, G., Paz-Ferreiro, J., Méndez, A., 2019. Thermogravimetric
546 analysis and carbon stability of chars produced from slow pyrolysis and
547 hydrothermal carbonization of manure waste. J. Anal. Appl. Pyrolysis 140, 434–
548 443. https://doi.org/10.1016/j.jaap.2019.04.026

549 Chen, H., Rao, Y., Cao, L., Shi, Y., Hao, S., Luo, G., Zhang, S., 2019. Hydrothermal
550 conversion of sewage sludge : Focusing on the characterization of liquid products
551 and their methane yields. Chem. Eng. J. 357, 367–375.
552 https://doi.org/10.1016/j.cej.2018.09.180

553 Cherrier, V., Grebot, B., Kirhensteine, I., Brutus, K., Berman, S., Sarteel, M., 2014.

554 Collection and analysis of data for the control of emissions from the spreading of
555 manure, European commission, AMEC Environment & Infracstructure UK
556 Limited.
557 Dai, L., Yang, B., Li, H., Tan, F., Zhu, N., Zhu, Q., He, M., Ran, Y., Hu, G., 2017. A
558 synergistic combination of nutrient reclamation from manure and resultant
559 hydrochar upgradation by acid-supported hydrothermal carbonization. Bioresour.
560 Technol. 243, 860–866. https://doi.org/10.1016/j.biortech.2017.07.016
561 De la Rubia, M.A., Villamil, J.A., Rodriguez, J.J., Borja, R., Mohedano, A.F., 2018a.
562 Mesophilic anaerobic co-digestion of the organic fraction of municipal solid waste
563 with the liquid fraction from hydrothermal carbonization of sewage sludge. Waste
564 Manag. 76, 315–322. https://doi.org/10.1016/j.wasman.2018.02.046
565 De la Rubia, M.A., Villamil, J.A., Rodriguez, J.J., Mohedano, A.F., 2018b. Effect of
566 inoculum source and initial concentration on the anaerobic digestion of the liquid
567 fraction from hydrothermal carbonisation of sewage sludge. Renew. Energy 127,
568 697–704. https://doi.org/10.1016/j.renene.2018.05.002
569 Dubois, M., Gilles, K.A., Hamilton, J.K., Rebers, P.A., Smith, F., 1956. Colorimetric
570 method for determination of sugars and related substances. Anal. Chem 28, 350–
571 356.
572 EBA, 2017. Annual statistical report of the European biogas association.
573 Ecoprog, 2017. The Market for Mechanical Biological Waste Treatment in Europe.
574 Ekpo, U., Ross, A.B., Camargo-valero, M.A., Fletcher, L.A., 2016. Bioresource
575 Technology Influence of pH on hydrothermal treatment of swine manure : Impact
576 on extraction of nitrogen and phosphorus in process water. Bioresour. Technol.
577 214, 637–644. https://doi.org/10.1016/j.biortech.2016.05.012
578 EN 15400:2011, 2011. Solid recovered fuels – determination of calorific value. CEN

579 Eur. CS, Brussels.
580 Gao, Y., Liu, Y., Zhu, G., Xu, J., Yuan, Q., Zhu, Y., Sarma, J., Wang, Y., Wang, J., Ji,
581 L., 2018. Microwave-assisted hydrothermal carbonization of dairy manure :
582 Chemical and structural properties of the products. Energy 165, 662–672.
583 https://doi.org/10.1016/j.energy.2018.09.185
584 Gascó, G., Paz-ferreiro, J., Álvarez, M.L., Saa, A., Méndez, A., 2018. Biochars and
585 hydrochars prepared by pyrolysis and hydrothermal carbonisation of pig manure
586 79, 395–403. https://doi.org/10.1016/j.wasman.2018.08.015
587 Ghanim, B.M., Shankar, D., Kwapinski, W., Leahy, J.J., 2016. Hydrothermal
588 carbonisation of poultry litter : Effects of treatment temperature and residence time
589 on yields and chemical properties of hydrochars. Bioresour. Technol. 216, 373–
590 380. https://doi.org/10.1016/j.biortech.2016.05.087
591 Huang, R., Fang, C., Zhang, B., Tang, Y., 2018. Transformations of phosphorus
592 speciation during (hydro) thermal treatments of animal manures. Environ. Sci.
593 Technol 52, 3016–3026. https://doi.org/10.1021/acs.est.7b05203
594 Jain, S., Sharma, M.P., 2011. Power generation from MSW of Haridwar city: A
595 feasibility study. Renew. Sustain. Energy Rev. 15, 69–90.
596 https://doi.org/10.1016/j.rser.2010.09.007
597 Lang, Q., Guo, Y., Zheng, Q., Liu, Z., Gai, C., 2018. Co-hydrothermal carbonization of
598 lignocellulosic biomass and swine manure: Hydrochar properties and heavy metal
599 transformation behavior. Bioresour. Technol. 266, 242–248.
600 https://doi.org/10.1016/j.biortech.2018.06.084
601 Lang, Q., Zhang, B., Liu, Z., Chen, Z., Xia, Y., Li, D., Ma, J., 2019a. Co-hydrothermal
602 carbonization of corn stalk and swine manure: Combustion behavior of hydrochar
603 by thermogravimetric analysis. Bioresour. Technol. 271, 75–83.

https://doi.org/10.1016/j.biortech.2018.09.100

Lang, Q., Zhang, B., Liu, Z., Jiao, W., Xia, Y., Chen, Z., 2019b. Properties of hydrochars derived from swine manure by CaO assisted hydrothermal carbonization. J. Environ. Manage. 233, 440–446. https://doi.org/10.1016/j.jenvman.2018.12.072

Liu, Ziyun, Zhang, Y., Liu, Zhidan, 2019. Comparative production of biochars from corn stalk and cow manure. Bioresour. Technol. 291, 121855. https://doi.org/10.1016/j.biortech.2019.121855

Ma, B., Li, X., Xu, L., Wang, K., Wang, X., 2006. Investigation on catalyzed combustion of high ash coal by thermogravimetric analysis. Thermochim. Acta 445, 19–22. https://doi.org/10.1016/j.tca.2006.03.021

Marin-Batista, J., Villamil, J.A., Rodriguez, J.J., Mohedano, A.F., Rubia, M.A. De, 2019. Valorization of microalgal biomass by hydrothermal carbonization and anaerobic digestion. Bioresour. Technol. 274, 395–402. https://doi.org/10.1016/j.biortech.2018.11.103

Mostafa Imeni, S., Pelaz, L., Corchado-lopo, C., Busquets, A.M., Ponsá, S., Colón, J., 2019. Techno-economic assessment of anaerobic co-digestion of livestock manure and cheese whey (Cow , Goat & Sheep) at small to medium dairy farms. Bioresour. Technol. 291, 121872. https://doi.org/10.1016/j.biortech.2019.121872

Niu, S., Chen, M., Li, Y., Xue, F., 2016. Evaluation on the oxy-fuel combustion behavior of dried sewage sludge. Fuel 178, 129–138. https://doi.org/10.1016/j.fuel.2016.03.053

Passos, F., Ortega, V., Donoso-bravo, A., 2017. Thermochemical pretreatment and anaerobic digestion of dairy cow manure: Experimental and economic evaluation. Bioresour. Technol. 227, 239–246. https://doi.org/10.1016/j.biortech.2016.12.034

629 Randall, R.J., Lewis, a, 1951. The folin by oliver. Readings 193, 265–275.
630 https://doi.org/10.1016/0304-3894(92)87011-4
631 Raposo, F., de la Rubia, M.A., Borja, R., Alaiz, M., 2008. Assessment of a modified
632 and optimised method for determining chemical oxygen demand of solid substrates
633 and solutions with high suspended solid content. Talanta 76, 448–453.
634 https://doi.org/10.1016/j.talanta.2008.03.030
635 Raposo, F., Fernández-Cegrí, V., De la Rubia, M.A., Borja, R., Béline, F., Cavinato, C.,
636 Demirer, G., Fernández, B., Fernández-Polanco, M., Frigon, J.C., Ganesh, R.,
637 Kaparaju, P., Koubova, J., Méndez, R., Menin, G., Peene, A., Scherer, P., Torrijos,
638 M., Uellendahl, H., Wierinck, I., de Wilde, V., 2011. Biochemical methane
639 potential (BMP) of solid organic substrates: Evaluation of anaerobic
640 biodegradability using data from an international interlaboratory study. J. Chem.
641 Technol. Biotechnol 86, 1088–1098.
642 Reza, M.T., Mumme, J., Ebert, A., 2015. Characterization of hydrochar obtained from
643 hydrothermal carbonization of wheat straw digestate 425–435.
644 https://doi.org/10.1007/s13399-015-0163-9
645 Smith, A.M., Singh, S., Ross, A.B., 2016. Fate of inorganic material during
646 hydrothermal carbonisation of biomass : Influence of feedstock on combustion
647 behaviour of hydrochar. FUEL 169, 135–145.
648 https://doi.org/10.1016/j.fuel.2015.12.006
649 Smith, A.M., Whittaker, C., Shield, I., Ross, A.B., 2018. The potential for production of
650 high quality bio-coal from early harvested Miscanthus by hydrothermal
651 carbonisation. Fuel 220, 546–557. https://doi.org/10.1016/j.fuel.2018.01.143
652 Tavasoli, A., Aslan, M., Salimi, M., Balou, S., Pirbazari, S.M., Hashemi, H., Kohansal,
653 K., 2018. Influence of the blend nickel/porous hydrothermal carbon and cattle

manure hydrochar catalyst on the hydrothermal gasification of cattle manure for H2 production. Energy Convers. Manag. 173, 15–28. https://doi.org/10.1016/j.enconman.2018.07.061

Toufiq Reza, M., Freitas, A., Yang, X., Hiibel, S., Lin, H., Coronella, C.J., 2016. Hydrothermal Carbonization (HTC) of Cow Manure: Carbon and Nitrogen Distributions in HTC Products. Environ. Prog. Sustain. Energy 35, 1002–1011. https://doi.org/10.1002/ep

Toufiq Reza, M., Poulson, S.R., Román, S., Coronella, C.J., 2018. Behavior of Stable Carbon and Stable Nitrogen Isotopes during Hydrothermal Carbonization of biomass. J. Anal. Appl. Pyrolysis 131, 85–92. https://doi.org/10.1016/j.jaap.2018.02.006

Villamil, J.A., Mohedano, A.F., Martín, J.S., Rodriguez, J.J., Rubia, M.A. De, 2020. Anaerobic co-digestion of the process water from waste activated sludge hydrothermally treated with primary sewage sludge . A new approach for sewage sludge management. Renew. Energy 146, 435–443. https://doi.org/10.1016/j.renene.2019.06.138

Villamil, J.A., Mohedano, A.F., Rodriguez, J.J., de la Rubia, M.A., 2018. Valorisation of the liquid fraction from hydrothermal carbonisation of sewage sludge by anaerobic digestion. J. Chem. Technol. Biotechnol. 93, 450–456. https://doi.org/10.1002/jctb.5375

Villamil, J.A., Mohedano, A.F., Rodriguez, J.J., Rubia, M.A. De, 2019. Anaerobic co-digestion of the aqueous phase from hydrothermally treated waste activated sludge with primary sewage sludge . A kinetic study. J. Environ. Manage. 231, 726–733. https://doi.org/10.1016/j.jenvman.2018.10.031

Wang, L., Zhang, L., Li, A., 2014. Hydrothermal treatment coupled with mechanical

679 expression at increased temperature for excess sludge dewatering: Influence of
680 operating conditions and the process energetics. Water Res. 65, 85–97.
681 https://doi.org/10.1016/j.watres.2014.07.020
682 Ware, A., Power, N., 2017. Modelling methane production kinetics of complex poultry
683 slaughterhouse wastes using sigmoidal growth functions. Renew. Energy 104, 50–
684 59.
685 Wu, K., Gao, Y., Zhu, G., Zhu, J., Yuan, Q., Chen, Y., 2017. Characterization of dairy
686 manure hydrochar and aqueous phase products generated by hydrothermal
687 carbonization at di ff erent temperatures. J. Anal. Appl. Pyrolysis 127, 335–342.
688 https://doi.org/10.1016/j.jaap.2017.07.017
689 Wu, K., Zhang, X., Yuan, Q., 2018. Effects of process parameters on the distribution
690 characteristics of inorganic nutrients from hydrothermal carbonization of cattle
691 manure 209, 328–335. https://doi.org/10.1016/j.jenvman.2017.12.071
692 Xiong, J., Pan, Z., Xiao, X., Huang, H., Lai, F., Wang, J., Chen, S., 2019. Study on the
693 hydrothermal carbonization of swine manure: The effect of process parameters on
694 the yield/ properties of hydrochar and process water. J. Anal. Appl. Pyrolysis 144,
695 104692. https://doi.org/10.1016/j.jaap.2019.104692
696 Zhang, D., Wang, F., Shen, X., Yi, W., Li, Z., Li, Y., 2018. Comparison study on fuel
697 properties of hydrochars produced from corn stalk and corn stalk digestate. Energy
698 165, 527–536. https://doi.org/10.1016/j.energy.2018.09.174
699 Zhao, C., Yan, H., Liu, Y., Huang, Y., Zhang, R., Chen, C., Liu, G., 2016. Bio-energy
700 conversion performance, biodegradability, and kinetic analysis of different fruit
701 residues during discontinuous anaerobic digestion. Waste Manag. 52, 295–301.
702 Zhou, S., Liang, H., Han, L., Huang, G., Yang, Z., 2019. The influence of manure
703 feedstock , slow pyrolysis , and hydrothermal temperature on manure

704 thermochemical and combustion properties. Waste Manag. 88, 85–95.
705 https://doi.org/10.1016/j.wasman.2019.03.025
706